Acta Neuropathologica Communications

RESEARCH

Open Access

JMJD3 deficiency disturbs dopamine biosynthesis in midbrain and aggravates chronic inflammatory pain

Xi-Biao He[1*], Fang Guo[1†], Wei Zhang[2†], Jiacheng Fan[1], Weidong Le[3], Qi Chen[1], Yongjun Ma[1,7], Yong Zheng[1], Sang-Hun Lee[4], Hui-Jing Wang[5], Yi Wu[1,8], Qinming Zhou[6] and Rui Yang[1]

Abstract

Midbrain dopamine (mDA) neurons participate in a wide range of brain functions through an intricate regulation of DA biosynthesis. The epigenetic factors and mechanisms in this process are not well understood. Here we report that histone demethylase JMJD3 is a critical regulator for DA biosynthesis in adult mouse mDA neurons. Mice carrying *Jmjd3* conditional knockout or undergoing pharmaceutical inhibition of JMJD3 showed consistent reduction of DA content in midbrain and striatum. Histological examination of both mice confirmed that TH and NURR1, two key molecules in DA biosynthesis pathway, were decreased in mDA neurons. Mechanistic experiments in vivo and in vitro further demonstrated that the transcriptions of *Th* and *Nurr1* in mDA neurons were suppressed by JMJD3 deficiency, because of increased repressive H3K27me3 and attenuated bindings of JMJD3 and NURR1 on the promoters of both genes. On behavioral level, a significant prolonged inflammation-induced mechanical hyperalgesia was found in conditional knockout mice regardless of sex and age, whereas motor function appeared to be intact. Our findings establish a novel link between DA level in mDA neurons with intrinsic JMJD3 activity, and suggest prolonged chronic inflammatory pain as a major loss-of-function consequence.

Keywords Dopamine biosynthesis, Midbrain dopamine neuron, Transcriptional regulation, Chronic inflammatory pain, Epigenetic control

†Fang Guo and Wei Zhang contributed equally to this work.

*Correspondence:
Xi-Biao He
hexb@sumhs.edu.cn
[1]Laboratory of Stem Cell Biology and Epigenetics, School of Basic Medical Sciences, Shanghai University of Medicine & Health Sciences, 279 Zhouzhu Highway, Pudong New Area, Shanghai 201318, China
[2]State Key Laboratory of Microbial Metabolism, School of Life Science and Biotechnology, Shanghai Jiao Tong University, Shanghai 200240, China
[3]Center for Translational Medicine, Shanghai University of Medicine & Health Sciences, Shanghai 201318, China
[4]Department of Biochemistry and Molecular Biology, College of Medicine, Hanyang University, Seoul, Republic of Korea
[5]Laboratory of Neuropsychopharmacology, School of Basic Medical Sciences, Shanghai University of Medicine & Health Sciences, Shanghai 201318, China
[6]Department of Neurology, Ruijin Hospital, Shanghai Jiao Tong University School of Medicine, Shanghai 200025, China
[7]The Interdisciplinary Research Center of Biology and Chemistry, Chinese Academy of sciences, Shanghai 200120, China
[8]Institute of Neuroscience, State Key Laboratory of Neuroscience, CAS Center for Excellence in Brain Science and Intelligence Technology, Chinese Academy of Sciences, Shanghai 200031, China

Introduction

Midbrain dopamine (mDA) neurons are the main producer of neurotransmitter DA in the adult central nervous system (CNS) and participate in the regulation of a wide range of brain functions including locomotion, cognition, emotion and reward [1]. The biosynthesis of DA in mDA neurons is biochemically controlled by its rate-limiting enzyme tyrosine hydroxylase (TH) [2], which plays essential roles in both fetal development and adult brain [3–5]. Dysregulation of TH in catecholamine (CA) neurons including mDA neurons has been linked to various brain pathologies such as neurotoxicity [6], depression [7] and Parkinson's disease (PD) [4, 5, 8].

The involvement of mDA transmission in the central regulation of pain is getting recognized [9–18]. In particular, inflammatory stimuli have been reported to directly down-regulate ventral tegmental area (VTA) DA activity and inhibit mesolimbic pathway, indicating VTA mDA neurons as a major mediator of chronic inflammatory pain [10, 19, 20]. Moreover, chronic pain is one of the most common non-motor symptoms in PD patients [21], suggesting an association between pain hyperactivity and DA neuropathology. However, the link between mDA biosynthesis pathway and chronic inflammatory pain remains to be established.

Depending on context, TH expression and activity are epigenetically, transcriptionally and post-translationally regulated [22]. The transcription of *Th* in developing mDA neurons is orchestrated by a large number of transcription factors and epigenetic modifications [23]. For instance, the transcription of *Th* that specifies the DA phenotype of developing mDA neurons is determined by both the transcription factor binding of Nuclear receptor-related factor 1 (NURR1) and alterations of several histone modifications and DNA methylation on *Th* promoter [24–27]. By contrast, relatively few epigenetic factors and corresponding regulatory mechanisms of TH expression thereby DA biosynthesis in adult mDA neurons have been elucidated.

Jumonji domain containing-3 (JMJD3) is a histone demethylase that specifically de-methylates histone 3 lysine 27 tri-methylation (H3K27me3), which is related to chromatin remodeling-induced gene re-activation [28]. JMJD3 is involved in a plethora of functions including, but not limited to embryonic development [26, 29, 30], inflammation [31–35], apoptosis [36] and cell senescence [37, 38] and has been associated with various diseases such as myocardial infarctions, Kawasaki disease, rheumatoid arthritis, and encephalomyelitis [39, 40]. Despite of its well-studied inflammatory regulation role in microglia [31, 33, 34], the roles of JMJD3 in other CNS cell types are largely unexplored.

In this study, by performing a series of biochemical, histological, cellular and behavioral experiments using conditional knockout (cKO) and pharmaceutical inhibition, we reveal that JMJD3 is a critical regulator of the DA output in adult mDA neurons and identify its potential correlation with chronic inflammatory pain.

Materials and methods

Ethics

All animal experiments were approved by the animal ethics committee of Shanghai University of Medicine & Health Sciences and have been performed in accordance with the ethical standards laid down in the 1964 Declaration of Helsinki and its later amendments.

Animals

For *Th*-specific *Jmjd3* cKO experiments, *Th*-CRE mice (C57BL/6 background) were crossbred with heterozygous floxed *Jmjd3* mice (C57BL/6 background; a kind gift from Dr. Degui Charlie Chen) to generate cKO mice, whereas littermates of *Th*-CRE were used as WT. As DA levels and regulation differ along age and sex, transgenic mice were sub-grouped into male and female, mature-adult (4–6 months old (mo)) and middle-aged (12–14 mo) [41]. For systemic JMJD3 inhibition experiments, 4 mo male and female C57BL/6 mice were used. GSK-J4 dissolved in dimethyl sulfoxide (DMSO) was daily injected intraperitoneally (i.p.) at 20 mg/kg body weight into mice for two or five consecutive days. For focal JMJD3 inhibition, GSK-J4 dissolved in DMSO was daily injected intrathecally (i.t.) at 20 mg/kg body weight into L4-L6 vertebral spine for five consecutive days. DMSO was injected in parallel as Vehicle. Sodium-dependent vitamin C transporter 2 (*Svct2)* KO mouse embryos (C57BL/6 background) at embryonic day 14.5 were kindly provided by Dr. Fiona E. Harrison and have been described in previous study [26]. All animals were housed under standard conditions with controlled 12-hour light/dark cycles with food and water provided ad libitum.

Immunofluorescence staining and microscopy

Brain tissues were pre-fixed with 4% paraformaldehyde (PFA) by cardiac perfusion and post-fixed for 3 h, dehydrated in 30% sucrose and stored in embedding compound (Tissue-Tek) at -80 °C until cryosection. Tissues were cryosectioned into 14 μm thickness (Leica CM1950). Cultured cells were fixed with 4% PFA for 20 min. For immunostaining, tissue slices or cultured cells were permeabilized and blocked with PBS with 0.3% TritonX-100 and 1% bovine serum albumin for 40 min, incubated with primary antibodies diluted in blocking solution at 4 °C overnight. Alexa Fluor series of second antibodies (Thermo Scientific) were applied for one hour at room temperature. Cells were finally counterstained with 4',6-diamidino-2-phenylindole (DAPI) and examined

using fluorescence microscope (Leica DMi8). The antibody information is listed in Supplemental Table 1 A.

High performance liquid chromatography-mass spectrometry (HPLC-MS) analysis

HPLC-MS experiments were performed as previously described [42, 43]. Briefly, samples from different brain regions after mouse sacrifice were homogenized in ice-cold 0.2 M perchloric acid/methanol, sonicated (Bioruptor) and centrifuged at 10,000 g for 20 min. Supernatants were then filtered through 0.22 μm filter and stored in -80 °C. At least four animals per genotype or drug treatment were used. Analytes were separated using a Model 1260 HPLC system consisting of a binary pump, on-line degasser, thermostated dual 54-well plate autosampler, and a thermosated column compartment (Agilent Technologies, Santa Clara, CA) with a Poroshell 120 SB-C18 reverse phase column (3.0×100 mm, 2.7 μm, particle size, Agilent Technologies, Santa Clara, CA) temperature-controlled at 25 ℃. The mobile phase consisted of A (1mM ammonium formate, 0.1% (v/v) formic acid and 1% (v/v) methanol in water) and B (1 mM ammonium formate 0.1% (v/v) formic acid and 0.9% (v/v) H_2O in methanol). The gradient conditions of the mobile phase were as follows: 0 min, 5% B; 20 min, 95% B; 21 min, 5% B and 28 min, 5% B. The flow rate of the mobile phase was 0.3 ml/min, and the injection volume was 10 μl. For MS analysis, LC flow was coupled to an Agilent model 6470 triple quadrupole MS (Agilent Technologies, Santa Clara, CA), equipped with an Agilent Jet Stream electrospray ionization source. The MS was operated with the following parameters: capillary voltage, 4000 V for positive and 3500 V for negative; nozzle voltage, 500 V. Nitrogen was used as the drying (5 L/min, 300 ℃), sheath (11 L/min, 250 ℃) and nebulizer gas (45 psi). The data was acquired using Agilent MassHunter Workstation Data Acquisition Software (revision B.04). Multiple-reaction-monitoring transitions parameters, such as precursor ions, product ions, fragmentor voltage, collision energy as well as polarity were shown in Supplemental Table 1B. For the compounds which had two product ions, it was shown that the product ion was used as quantitative ion or qualitative one. The dwell time was 50 ms for transitions.

Cell culture

Primary mDA neurons were cultured as previously described [26] with minor modifications. DA progenitors were extracted from embryonic day 11 ICR mouse ventral mesencephalon. At this stage, the substantia nigra pars compacta (SNc) and VTA are not anatomically or molecularly distinct [44, 45], enabling these cells differentiating into both DA subtypes. DA progenitors were mechanically dissociated into single cells and plated onto 24-well plates or 6-well dishes pre-coated with 15 μg/ml poly-L-ornithine and 1 μg/ml fibronectin. Cells were cultured in serum-free Neurobasal media supplemented with N2 and B27 supplements and 1% Penecillin/Streptomycin for 7 days to reach a complete DA neuronal differentiation. After that, 1 μM GSK-J4 or DMSO were treated for 24 h. DA neuronal cell line MES23.5 was cultured in Dulbecco's Modified Eagle Medium supplemented with 10% fetal bovine serum and 1% Penecillin/Streptomycin. All cells were incubated in 5% CO_2, 37 °C incubator.

Cell transfection

MES23.5 cells were transfected by the plasmid carrying human *Nurr1* gene (Miaoling Plasmid Sharing Platform plasmid #P21180) or empty control vector using Lipofectamine 2000 according to manufacturer's instructions. Cells were applied to downstream experiments 1.5 days after transfection.

Real-time PCR analysis

RNAs were extracted from cultured cells and tissues using RNA extraction kit and reverse transcribed into cDNAs (both from TAKARA) according manufacturer's instructions. Real-time PCR was performed on a Real-time system (Roche) using SYBR green supermix (Vazyme). The comparative cycle threshold method was used for quantification. Gene expression values were normalized to those of *Gapdh*. Primer sequences are listed in Supplemental Table 1 C.

Chromatin immunoprecipitation (ChIP) assay

ChIP experiments were performed as previously described [26]. In brief, cells were cross-linked with 1% PFA for 10 min and sonicated to shear chromatin into small fragments with an average length of 200–400 bp (Bioruptor). Immunoprecipitation antibodies are listed in Supplemental Table 1 A. Immunoprecipitated DNA fragments were collected by magnetic beads (Active Motif), purified, and subjected to real-time PCR using primers spanning 1 kilo bp of *Th* and *Nurr1* gene promoters. Data were normalized to values of the input DNA. Consensus NURR1 binding sites were identified using the Jaspar database (http://jaspar.genereg.net/).

Histone extraction and immunoblotting analysis

Tissues from spinal cords and dorsal root ganglia (DRG) fibers were extracted under a dissection microscope, homogenized, lysed and acid extracted overnight at 4 °C. The supernatants were quantified and underwent conventional Western blot procedure to separate and immunoblot the histones. Antibodies are listed in Supplemental Table 1 A.

Mechanical hyperalgesia test

Complete Freund's adjuvant (CFA)-induced chronic mechanical hyperalgesia was assessed as previously described [46]. Briefly, baseline responses were measured using von Frey's hairs (bending force range from 0.04 to 2.0 g, starting with 0.16 g; Stoelting) after mice were placed on a wire grid without receiving any nociceptive stimulation for 30 min. Next day, 20 µl CFA (Sigma-Aldrich) was injected intraplantarly, and the hyperalgesia responses were measured for various time points within 18 days. The hair force was increased or decreased according to the response, and the 50% paw withdrawal threshold was calculated using the up and-down method [47]. Nociceptive responses include clear paw withdrawal, shaking, and licking. Stimulus and measurement were repeated if ambiguous responses such as ambulation occurred.

Hargreaves test

Thermal algesia to noxious stimulus was measured using a hot/cold plate analgesia meter for mice (IITC) according to manufacturer's instructions. mice were put on a glass plate and the hind paw plantar surface was exposed to a beam of radiant heat (intensity latency 8–12 s) according to the Hargreaves method [48]. Latencies of hind paw withdrawal were recorded. The heat stimulation was repeated 2 times at an interval of 5 min for each mouse and the mean of both paws was calculated.

Accelerating rotarod test

The test was performed on a rotarod apparatus (IITC) according to manufacturer's manual. The 3 cm-diameter suspended rod was set to accelerate at a constant rate from 5 to 45 rpm in 240 s. Mice were pre-trained for 2 consecutive days before first trial. At each trial, mice were placed on the rod for a session of two repeats, with 180 s resting time allowed in between. A trial ended when the mouse fell off the rotarod or after reaching 240 s. Total four trials were performed for four consecutive days. The falling time was recorded and averaged of four trials.

Grip strength test

Hindlimb grip strength was measured with a grip strength meter for mice consisted of a T-shaped metal bar connected to a force transducer (IITC). Briefly, mice were held by tails allowing them to grasp the metal bar with hind paws, followed by a pulling of the mice backwards by the tail until grip was lost. The peak force was automatically recorded in grams (g) by the device. The measurement of grip strength was repeated 5 times at an interval of 5 min for each mouse and the mean was calculated.

Cell counting, immunoreactivity analysis and statistics

For in vivo immunoreactivity analysis, at least 50 TH+or NURR1+cells were counted in each brain region for one animal. Data were derived from three mouse brains of same experimental group and expressed as mean±SEM. The immunoreactivity of each cell was analyzed using ImageJ. For in vivo TH+or NURR1+cell number analysis, the total number of positive cells from sagittal sections containing VTA and SNc in one mouse brain was counted. To compensate the double counting in adjacent regions, the Abercrombie correction factor was introduced as following: [$N=n$ X (T/T+D)], in which N is the actual number of cells, n is the number of nuclear profiles, T is the section thickness, and D is the average diameter of nuclei. For in vitro analysis, cultured cells were counted in at least 10 random regions of each culture coverslip using an eyepiece grid at a magnification of 200 or 400X. Data are expressed as mean±SEM of three independent cultures. For HPLC-MS analysis, data were derived from four to seven mouse brains of same transgenic background and expressed as mean±SEM. Statistical comparisons were made using Student's t-test, one-way ANOVA with Tukey's post-hoc analysis and two-way ANOVA with Sidak's multiple comparisons test (Graphpad Prism 8.0).

Results

JMJD3 is highly expressed in the mDA neurons of adult mouse

We first investigated CA neuron-specific expression pattern of JMJD3 in adult mouse brains by performing whole-brain immunofluorescent co-labeling analysis of JMJD3 and TH, the rate-limiting enzyme catalyzing CA biosynthesis. Amongst 16 groups of TH+CA neurons, retrorubral field (RRF; A8), SNc (A9) and VTA (A10) are enriched with mDA neurons [2]. We found that JMJD3 was expressed exclusively in the nuclei of all the TH+mDA neurons in RRF, SNc and VTA (Fig. 1A). Similar expression pattern was observed in other TH+DA neurons including those in the arcuate nucleus of hypothalamus (A12), zona incerta (A13), hypothalamic preoptic area (A14/A15) and the glomerular layer of olfactory bulb (A16) (Fig. 1B). In addition, the TH+norepinephrine (NE) neurons in locus coeruleus (A6) were also enriched with nuclear JMJD3 (Fig. 1C). In the peripheral nervous system, TH is also expressed by a small population of DRG neurons responsible for injury-induced mechanical hypersensitivity that are known as C-low threshold mechanoreceptor (C-LTMR) [49, 50]. Interestingly, these cells expressed JMJD3 largely in the cell cytoplasm (Fig. 1D). Taken together, these results demonstrate a distinguished expression pattern of JMJD3 in the CA neurons of CNS.

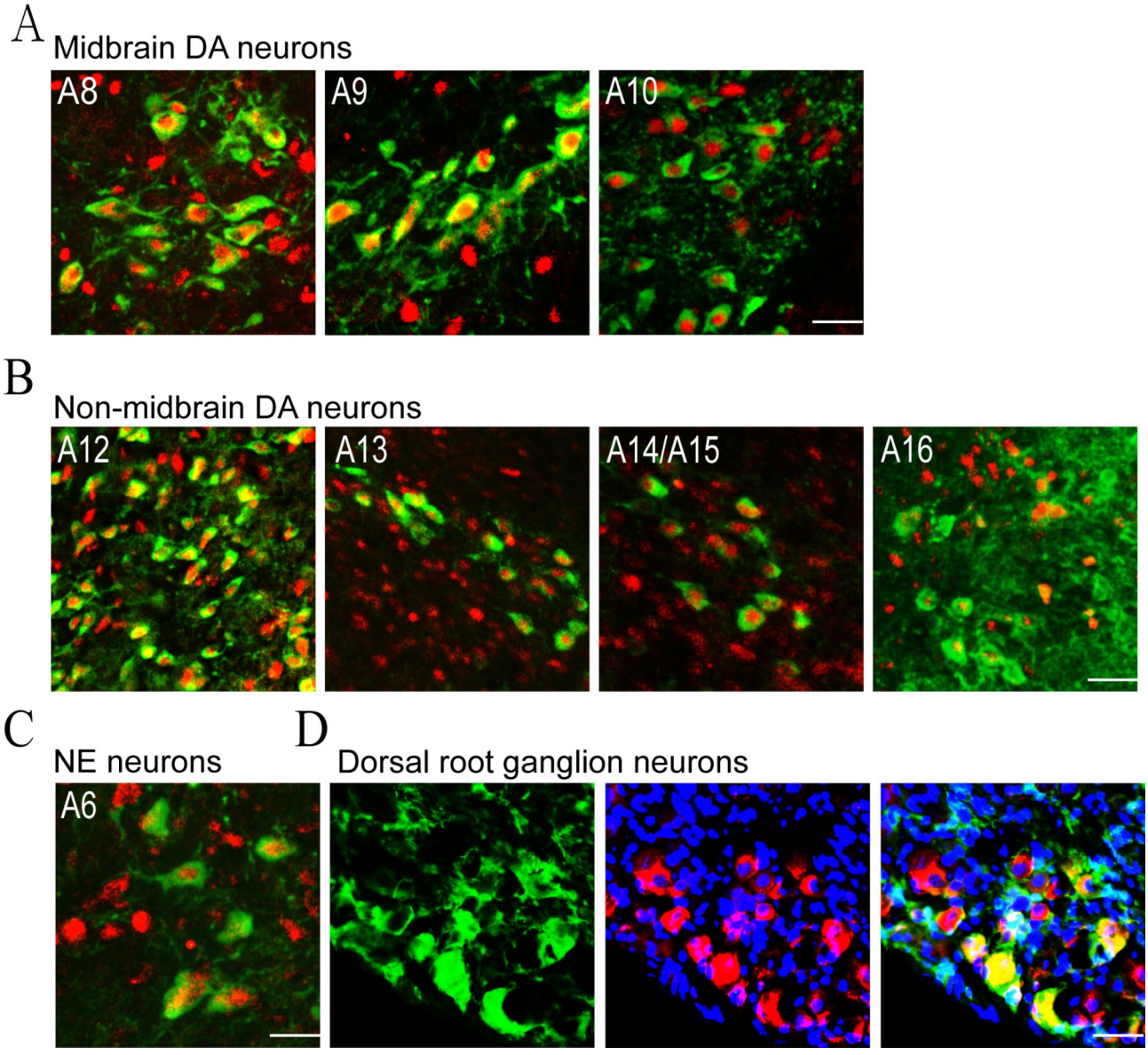

Fig. 1 JMJD3 expression in tyrosine hydroxylase (TH) + neurons in the central and peripheral nervous systems. Immunofluorescence co-labeling of TH (green) and JMJD3 (red) in midbrain dopamine (DA) neurons (**A**), non-midbrain DA neurons (**B**), norepinephrine (NE) neurons in locus coeruleus (**C**) and C-LTMR neurons in dorsal root ganglion (**D**) from 8-week-old C57BL/6 mice. Cell nuclei were counterstained by 4′,6-diamidino-2-phenylindole (blue). Scale bar represents 20 μm

Loss of JMJD3 reduces DA contents in the midbrain and striatum

To investigate the role of JMJD3 in adult mDA neurons, we created a heterozygous cKO mouse model by cross-breeding transgenic mice carrying *Th*-CRE and loxP-floxed *Jmjd3* loci. Offsprings carrying *Th*-CRE and one allele of loxP-floxed *Jmjd3* were used as cKO and littermates carrying *Th*-CRE and normal *Jmjd3* as control (WT; Suppl Fig. 1A). Immunohistochemistry showed a significantly reduced JMJD3 expression in the TH + mDA neurons of heterozygous cKO mice (Suppl Fig. 1B), accounting for about 40% loss of JMJD3 in the ventral midbrain as quantified by Western blot analysis (Suppl Fig. 1C). Therefore, all the following experiments were performed using heterozygous rather than homozygous cKO mice to avoid unnecessary animal sacrifice. To distinguish the source of CA contents, mouse brains were separated into several anatomical regions including frontal cortex, striatum, midbrain, cerebellum and brainstem, and the levels of DA and NE were measured by HPLC-MS. We found that the levels of DA in the midbrain and striatum of cKO mice were significantly lower than those of WT mice of both sexes, whereas no significant difference was observed in the frontal cortex, cerebellum or

brainstem (Fig. 2A and Suppl Fig. 2A). By contrast, the levels of NE in any brain regions above were not different between WT and cKO (Fig. 2B and Suppl Fig. 2B).

To confirm the results above, GSK-J4, a brain-penetrating small molecule inhibitor of JMJD3 [51], was daily i.p. injected into adult male mice for five days, followed by the same experimental procedure of HPLC-MS. In line with the results of cKO mice, levels of DA but not NE were specifically reduced in the midbrain and striatum of GSK-J4 mice (Fig. 2C, D), therefore providing consistent evidence supporting the specificity and vulnerability of mDA content to the disturbance of JMJD3 activity.

TH and NURR1, key factors for DA biosynthesis, are decreased in JMJD3-deficient mDA neurons

The biochemical findings above suggested that the DA biosynthesis in adult mDA neurons might be regulated by JMJD3. We therefore examined the TH expression in the SNc and VTA between WT and cKO by immunohistochemistry (Fig. 3A). In both regions, the TH immunoreactivities of cKO were significantly lower than those of WT (Fig. 3B). Of note, the total amounts of cells expressing TH were also lower in SNc and VTA of cKO mice, likely due to an over-reduced TH immunoreactivity rather than a loss of mDA neurons per se, as no sign of cell death or abnormal morphology was observed (Suppl Fig. 3). Consistently, the TH immunoreactivities were also decreased in the SNc and VTA of GSK-J4 mice, whereas small but statistically insignificant difference of total TH+cell number in either region was observed (Fig. 3C). These results provide histochemical evidence suggesting a suppression of TH by loss of JMJD3 in adult mDA neurons.

Given the essential role of transcription factor NURR1 in the maintenance of TH expression and DA function in adult mDA neurons [52–55], we further asked whether the protein expression of NURR1 was altered in cKO and GSK-J4 mice. As expected, either cKO or GSK-J4 caused remarkable decreases of NURR1 in the nuclei of TH+mDA neurons in SNc and VTA (Fig. 3D, E). To confirm this, we recruited a previously reported [26] mouse model of indirect JMJD3 inhibition in which JMJD3 activity is prohibited through genetic loss of vitamin C transporter gene *Svct2*. Although *Svct2* KO resulted in the agenesis of majority of mDA neurons, a small number of mDA progenitors were still able to migrate and differentiate into mDA neurons with reduced expression of TH in the mantle zone of embryonic ventral mesencephalon [26]. In these differentiated mDA neurons, the proportion that expressed NURR1 and the NURR1 immunoreactivity were both significantly lower in comparison to those of *Svct2* wildtype (Fig. 3F). Collectively, these results demonstrated that the expressions of TH and NURR1, two key molecules in the DA biosynthesis pathway, were both suppressed in mDA neurons lack of JMJD3.

JMJD3 directly activates *Th* and *Nurr1* transcription in mDA neurons

The nuclear expression of JMJD3 in mDA neurons suggests that TH and NURR1 might be transcriptionally regulated. To validate this, the transcriptional expressions of *Jmjd3*, *Th* and *Nurr1* genes in WT and cKO mice were examined by real-time PCR analysis. In comparison to WT, all three genes were down-regulated in the midbrain and striatum of JMJD3 cKO mice (Fig. 4A). To confirm

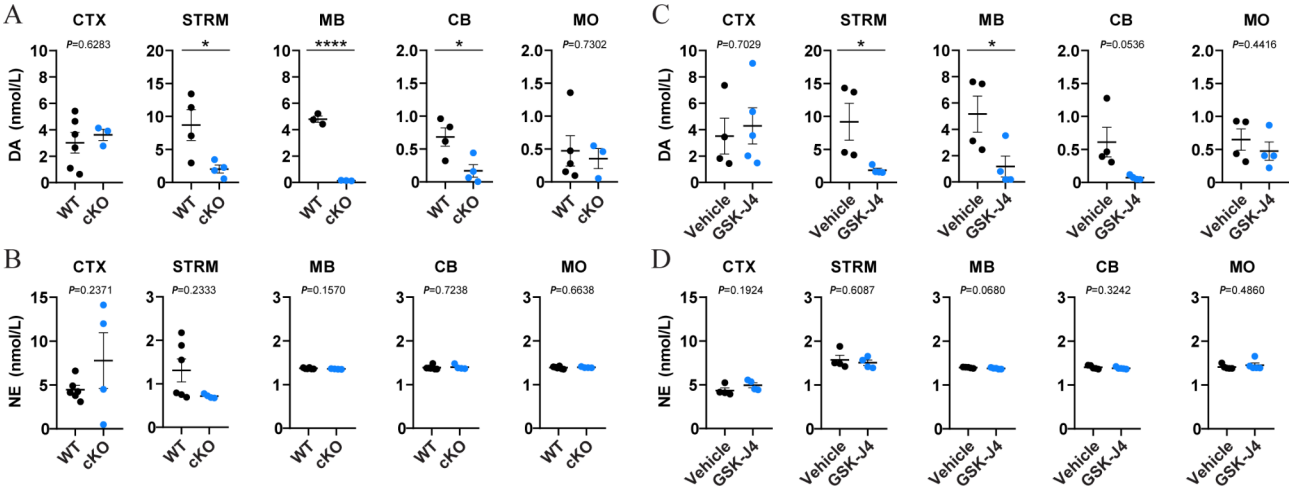

Fig. 2 Dopamine (DA) levels are decreased in the midbrain and striatum of two mouse models of JMJD3 deficiency. Brain tissues from the frontal cortex (CTX), striatum (STRM), midbrain (MB), cerebellum (CB) and medulla oblongata (MO) were micro-dissected, homogenized and the contents of DA and norepinephrine (NE) were measured by high performance liquid chromatography-mass spectrometry. (**A**, **B**) 4-month-old male conditional knockout (cKO) mice and their control littermates (WT). (**C**, **D**) 4-month-old male C57BL/6 mice underwent 5 consecutive days of intraperitoneal injection of GSK-J4 (20 mg/kg daily). In parallel, dimethyl sulfoxide was injected as Vehicle. $N = 4–7$ mice. Data represent mean ± SEM. *$P < 0.05$, ****$P < 0.0001$; Student's t-test

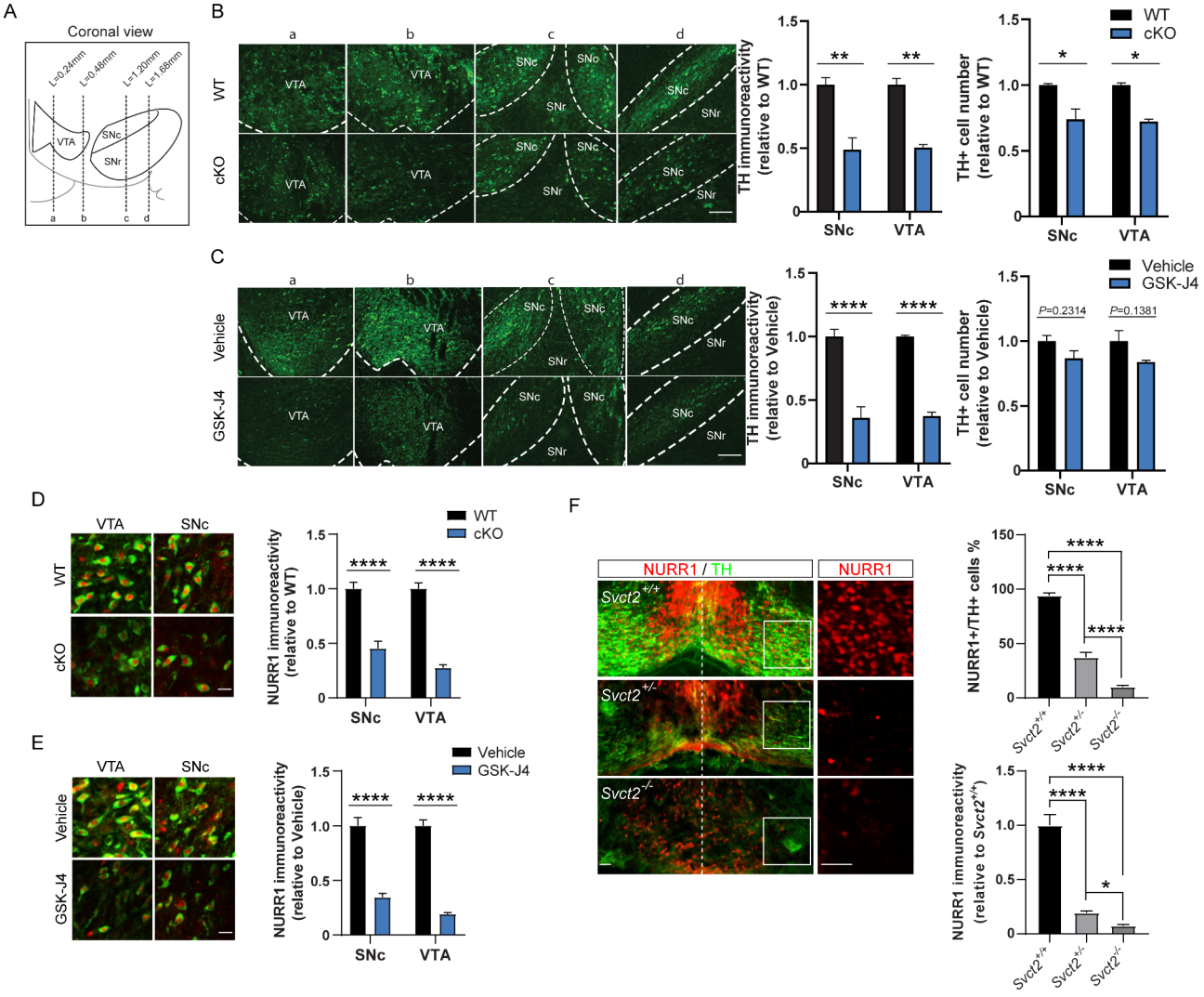

Fig. 3 Reduced expressions of tyrosine hydroxylase (TH) and NURR1 in midbrain dopamine (mDA) neurons of two JMJD3 deficiency mouse models. (**A**) Schematics showing the coronal view of the adult mouse midbrain compromised of ventral tegmental area (VTA), substantia nigra pars compacta (SNc) and pars reticulata (SNr). Dotted lines a-d indicate positions shown in B and C. (**B**) Left, representative immunofluorescence images of TH + mDA neurons in *Jmjd3* conditional knockout (cKO) mice and their control littermates (WT). Scale bar represents 100 μm. Right, quantifications of TH immunoreactivity and cell number of mDA neurons in VTA and SNc in WT and cKO mice. (**C**) Left, representative immunofluorescence images of TH + mDA neurons in GSK-J4 injected mice and their control (Vehicle). Scale bar represents 100 μm. Right, quantifications of TH immunoreactivity and cell number of DA neurons in VTA and SNc in GSK-J4 injected mice and control. (**D**, **E**) Representative immunofluorescence images and quantifications of NURR1 immunoreactivity showing decreased NURR1 (red) expression in TH + mDA neurons (green) in SNc and VTA of cKO and GSK-J4-injected mice in comparison to WT and Vehicle, respectively. Scale bar represents 20 μm. (**F**) Representative immunofluorescence images and quantifications showing effect of *Svct2* KO on TH and NURR1 expressions in mouse embryonic day 14.5 ventral mesencephalon. Insets show NURR1 expression in higher magnification. Scale bar represents 50 μm. For immunoreactivity analysis, at least 50 TH + cells from each mouse were measured and averaged. $N = 3–5$ mice. Data represent mean ± SEM. $^{*}P < 0.05$, $^{**}P < 0.01$, $^{****}P < 0.0001$; Student's t-test

this result in vitro, primary cultured mouse mDA neurons were challenged with GSK-J4 for 1 day. GSK-J4 remarkably reduced the number of cells expressing TH without affecting the total cell number, and the NURR1 immunoreactivity within TH+cells was also decreased (Fig. 4B). In consistent with in vivo data, the mRNA levels of both *Th* and *Nurr1* were down-regulated by GSK-J4 (Fig. 4C). Similar results were found in a GSK-J4-treated DA neuronal cell line MES23.5, in which TH was constitutively expressed [56] (Suppl Fig. 4A, B). A short hairpin RNA-mediated *Jmjd3* knockdown also significantly reduced TH protein and mRNA expressions, validating the specificity of GSK-J4 effect (Suppl Fig. 4C, D). Furthermore, overexpression of NURR1 failed to rescue GSK-J4- or short hairpin RNA-suppressed TH expression (Suppl Fig. 4E), indicating that JMJD3 expression is a prerequisite of NURR1-mediated *Th* gene transcription.

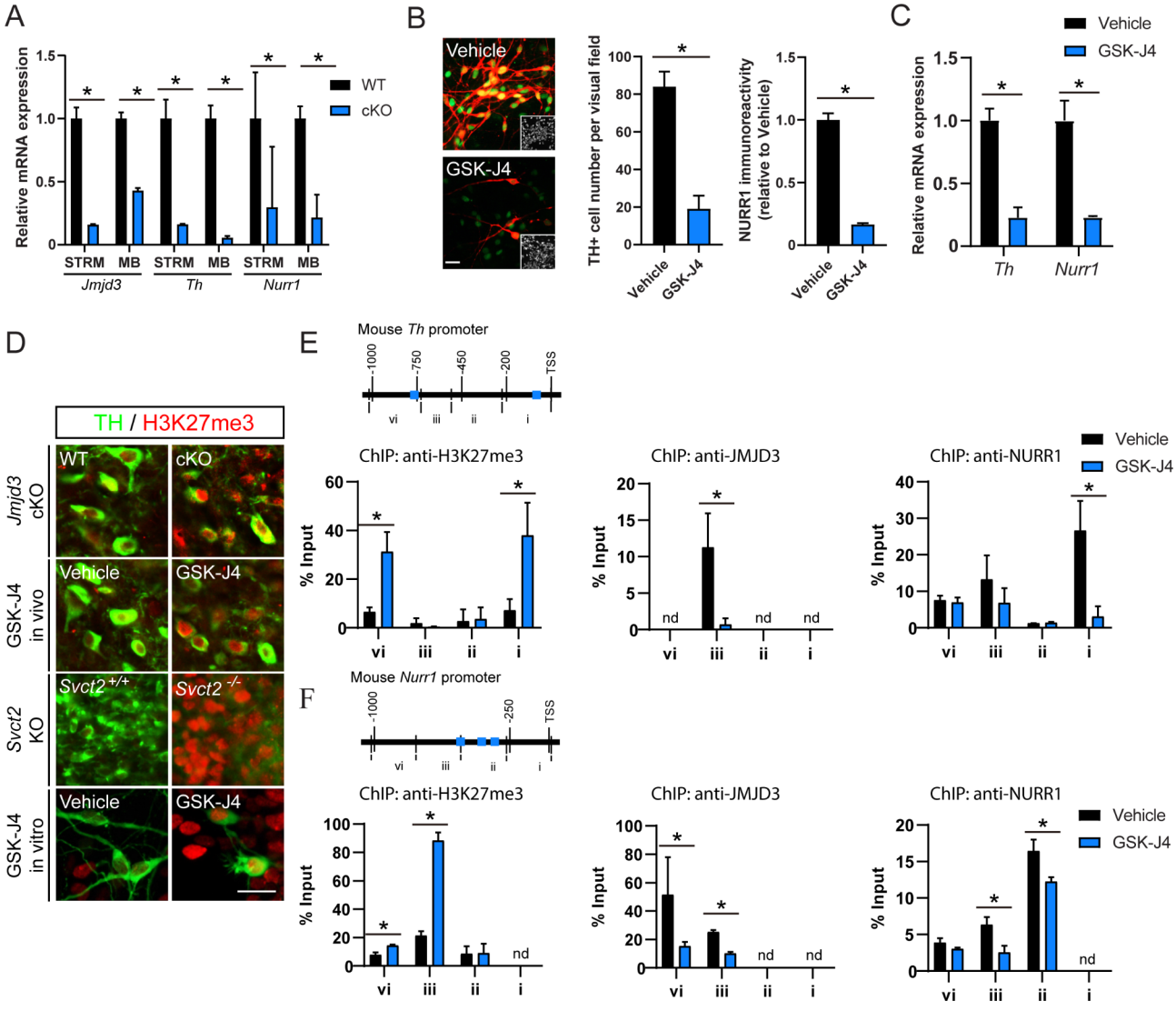

Fig. 4 Epigenetic control of *Th* and *Nurr1* gene transcription by JMJD3. (**A**) Real-time PCR analysis of mRNA levels of *Jmjd3*, *Th* and *Nurr1* from striatum (STRM) and midbrain (MB) in *Jmjd3* conditional knockout mice (cKO) and their control littermates (WT). *N* = 3 mice. Data represent mean ± SEM. (**B**) Representative immunofluorescence images and quantifications of NURR1 expression (green) in tyrosine hydroxylase (TH; red) + cells from primary culture of mouse midbrain dopamine (mDA) neurons with or without treatment of GSK-J4. Insets show cell nuclei. Scale bar represents 20 μm. (**C**) Real-time PCR analysis of *Th* and *Nurr1* mRNA levels in primary cultured mDA neurons after GSK-J4 treatment. (**D**) Representative immunofluorescence images of histone 3 lysine 27 tri-methylation (H3K27me3) in TH + mDA neurons from cKO, GSK-J4 mice, *Svct2* KO mouse embryos and primary cultured mDA neurons treated with GSK-J4. Scale bar represents 20 μm. (**E**, **F**) Chromatin immunoprecipitation (ChIP)-quantitative PCR analysis of H3K27me3, JMJD3 and NURR1enrichments on 1 kilo bp mouse *Th* (**E**) and *Nurr1* (**F**) promoters from DA neuronal cell line MES23.5 with or without GSK-J4 treatment. Blue boxes represent consensus NURR1 binding sites. Nd = not detected. *N* = 3 independent cell cultures. Data represent mean ± SEM. **P* < 0.05; Student's t-test and one-way ANOVA with Tukey's post-hoc test

As a chromatin modifier, JMJD3 binds to DNA and specifically de-methylates H3K27me3 [28]. Indeed, global increase of H3K27me3 was observed in mDA neurons from *Jmjd3* cKO, GSK-J4 mice and *Svct2* KO embryos, as well as in cultured mDA neurons treated with GSK-J4 (Fig. 4D). By performing ChIP assays using MES23.5 cells, we found that H3K27me3 was specifically induced by GSK-J4 within 1 kilo bp of both *Th* and *Nurr1* gene promoters (Fig. 4E, F), suggesting a chromatin remodeling of both genes by JMJD3. This was further supported by region-specific decreases of DNA bindings of JMJD3 induced by GSK-J4, within −745 to -475 bp of *Th* promoter (region iii), and −1091 to -510 bp of *Nurr1* promoter (region iii and vi), respectively. Moreover, the enrichments of NURR1 were also greatly decreased within 0 to -203 bp of *Th* promoter (region i) and within −298 to -847 bp of *Nurr1* promoter (region ii and iii; Fig. 4E, F), which correlated well with the locations of the consensus NURR1 binding site as previously reported [27]. Taken together, these results demonstrate that both

Nurr1 and *Th* promoters are directly targeted by JMJD3, lack of which leads to addition of repressive epigenetic mark and attenuated transactivation of both genes.

Jmjd3 cKO exaggerates chronic inflammatory pain

Next, we sought to establish connections between biochemical findings with behavioral consequences. As VTA DA activity is deeply involved in the neural circuit that mediates inflammatory and neuropathic pain [9, 10, 57], we hypothesized that the acute and chronic pain responses might be altered in *Jmjd3* cKO mice. To test this, 4–6 mo WT and cKO mice of both sexes underwent CFA-induced mechanical hyperalgesia and their acute and chronic pain responses were measured at various time points for 18 days by Von Frey's hairs (Fig. 5A).

WT and cKO mice of both sexes showed no difference in basal nociception without noxious stimulus (Suppl Fig. 5A). In WT mice of both sexes, significant pain hypersensitivity was induced by intraplanar injection of CFA within 3 h, maintained until the eighth day (D8),

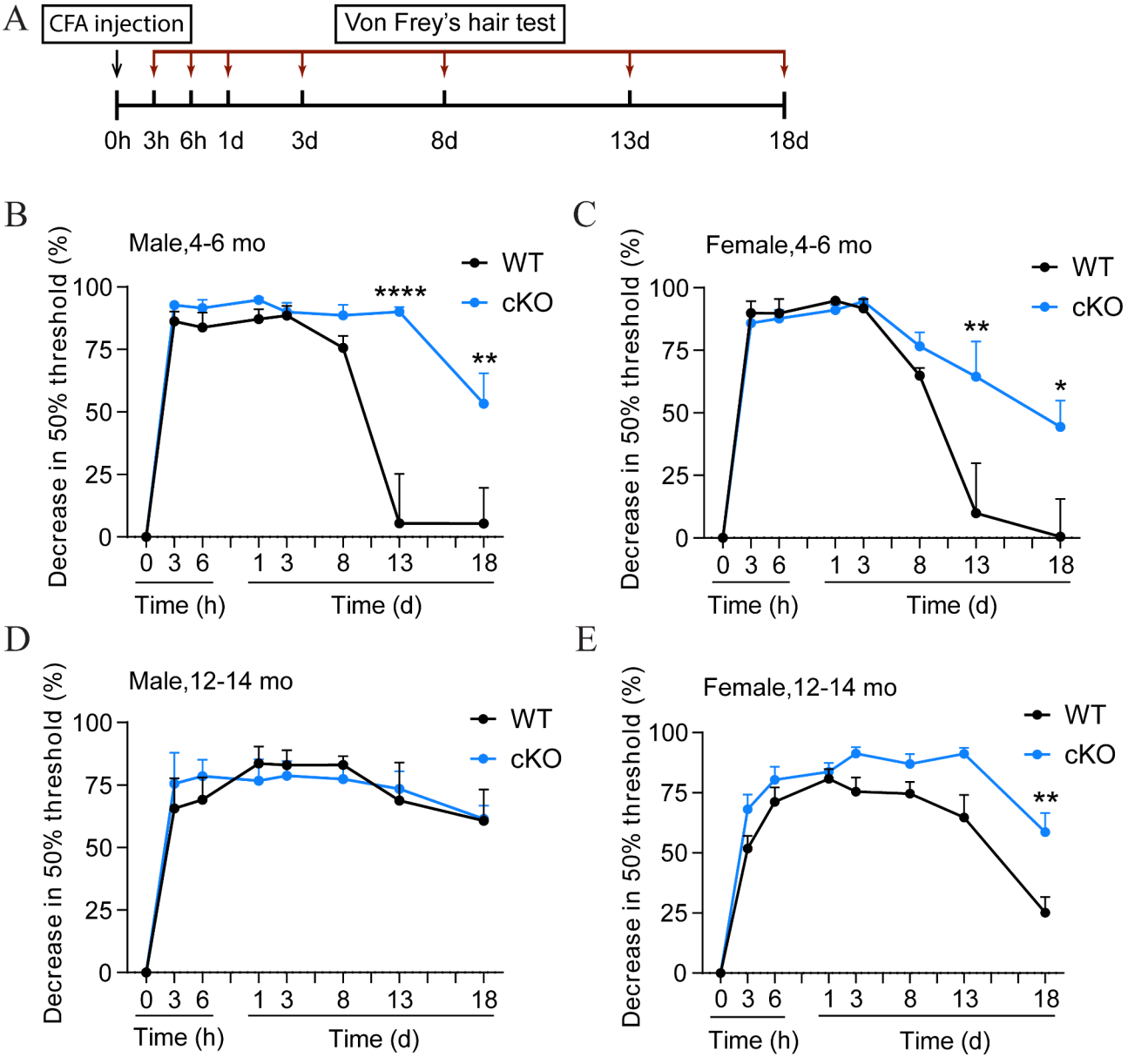

Fig. 5 Chronic inflammatory pain is exaggerated in *Jmjd3* conditional knockout (cKO) mice. (**A**) Schematics showing the experimental procedure for the assessment of complete Freund's adjuvant (CFA)-induced chronic inflammatory pain. Mice received an intraplantar injection of CFA and changes in 50% paw withdrawal threshold assessed by Von Frey's hair were monitored over 18 days. The CFA test was applied to male (**B**, **D**) and female (**C**, **E**) cKO mice and their control littermates (WT) at two different ages (mature-adult, 4–6 months old (mo) and middle-aged, 12–14 mo). Data represent mean ± SEM. $^{*}P < 0.05$, $^{**}P < 0.01$, $^{****}P < 0.0001$; two-way ANOVA with Sidak's multiple comparisons test

and gradually attenuated to a nearly complete recovery at D13, well validating the dynamics of chronic pain response to inflammatory stimulus. In comparison, CFA also induced remarkable pain hypersensitivity in cKO mice of both sexes within eight days. However, the hyperalgesia was maintained to D13, and was only slightly attenuated at D18 (Fig. 5B-C). To confirm the pain specificity, the thermal hyperalgesia was measured in parallel using a Hargreaves method [48] and no difference was observed (Suppl Fig. 5B). These results demonstrated a sex-independent prolonged chronic pain hypersensitivity by *Jmjd3* cKO.

Aging is a critical factor for chronic pain. To further explore the effect of aging on chronic pain response, the same CFA test was performed on 12–14 mo middle-aged WT and cKO mice. Interestingly, the hyperalgesia was not attenuated over 18 days after CFA injection in middle-aged male WT mice, and to a milder extent in middle-aged female ones, suggesting a further pain chronicity along aging. No difference of paw withdrawal was seen between male WT and cKO within 18 days, as both were still maintained at a hyperalgesia state (Fig. 5D). However, female cKO mice were significantly more sensitive than WT from D13 to D18 (Fig. 5E). Nevertheless, these results demonstrate that *Jmjd3* cKO causes age- and sex-independent chronic pain response to inflammatory stimulus.

TH + DRG neurons do not contribute to the pain effect of *Jmjd3* cKO

The fact that peripheral C-LTMR neurons in DRG also express TH raised concerns about their role in the pain effect observed above. To exclude this possibility, the CFA test was modified in which GSK-J4 was i.t. injected into the lumbar spines of 4 mo male and female mice daily from D8 to D12 to inhibit JMJD3 in C-LTMR DRG neurons (Fig. 6A). In parallel, mice of both sexes at same age were i.p. injected with GSK-J4 at D8 and D9 to induce mDA inhibition (Fig. 6B). 2 h after i.t. injection of GSK-J4, levels of H3K27m3 were increased in the lumbar spinal cords and DRG nerves of male and female mice (Suppl Fig. 5), confirming the focal inhibition of JMJD3. We found that i.t. injection of GSK-J4 for 5 days did not cause any alteration of pain response in either male or female mice, whereas i.p. injection of GSK-J4 for two days caused remarkable prolonged hyperalgesia (Fig. 6C, D). These data confirmed the involvement of mDA neurons and excluded that of peripheral DRG TH + neurons in chronic pain response.

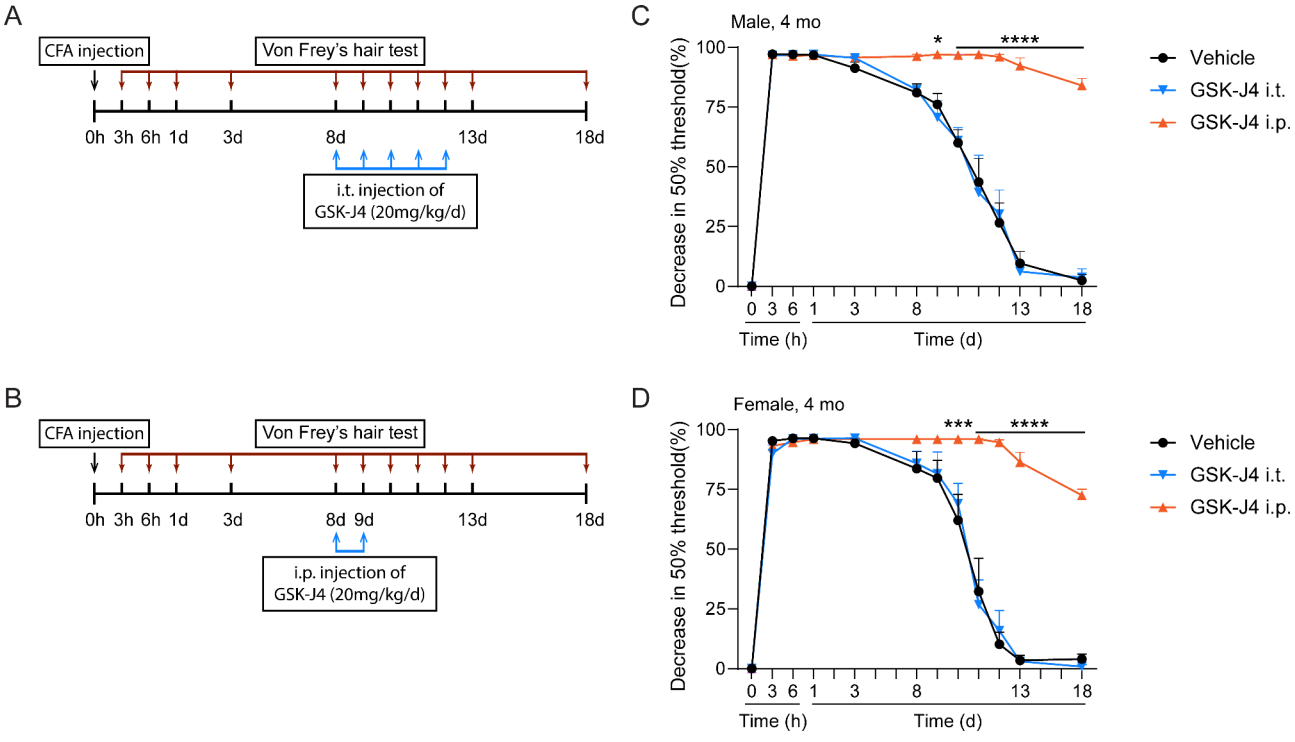

Fig. 6 Peripheral inhibition of JMJD3 does not affect chronic pain response. (**A**, **B**) schematics showing the modified experimental procedure based on the complete Freund's adjuvant (CFA)-induced chronic inflammatory pain. To induce peripheral inhibition of JMJD3, GSK-J4 was intrathecally (i.t.) injected during day 8 to day 13 into L4-L6 of 4-months old male and female C57BL/6mice (**A**). To induce temporary inhibition of JMJD3, GSK-J4 was intraperitoneally (i.p.) injected at day 8 and day 9 right before the pain recovery occurs (**B**). Dimethyl sulfoxide was injected as Vehicle. (**C**, **D**) No difference was found by peripheral inhibition of JMJD3 in male or female mice undergoing CFA-induced chronic inflammatory pain. *N* = 4 mice. Data represent mean ± SEM. Ns = not significant; two-way ANOVA with Sidak's multiple comparisons test

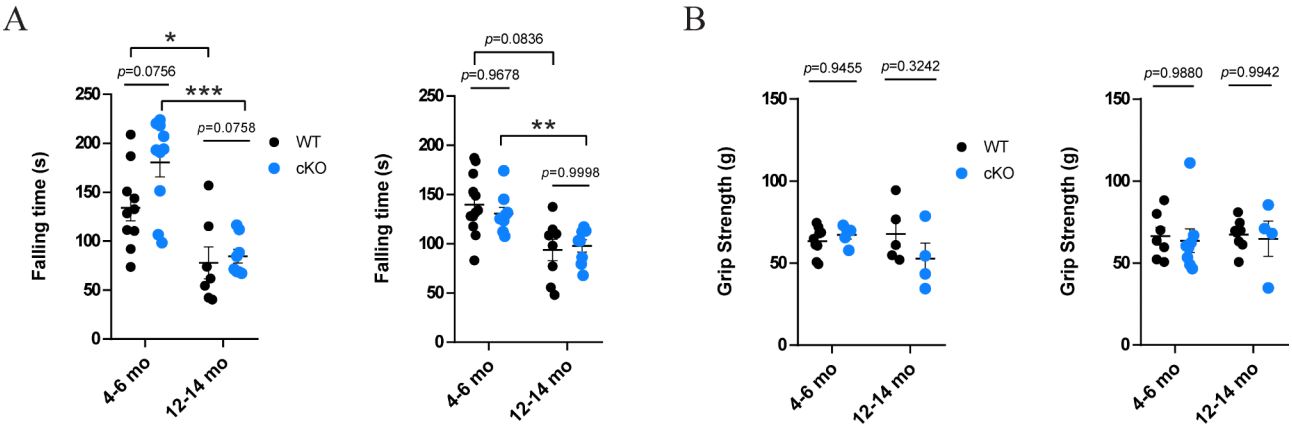

Fig. 7 Motor function is not affected in *Jmjd3* conditional knockout (cKO) mice. Mature-adult (4–6months old (mo)) and middle-aged (12–14 mo) cKO and WT mice were sub-grouped into male and female, applied to the accelerating rotarod test (**A**) and the grip strength test (**B**). $N = 4–10$ mice. Data represent mean ± SEM. $^{*}P < 0.05$, $^{**}P < 0.01$, $^{***}P < 0.001$. One- or two-way ANOVA with Tukey's post-hoc test or Sidak's multiple comparisons test

Motor function is not affected in *Jmjd3* cKO mice

We further investigated whether motor function, which is greatly affected by SNc DA activity, is affected by *Jmjd3* cKO. To test this, the accelerating rotarod test [58–61] and grip strength test were applied on mature-adult and middle-aged WT and cKO mice of both sexes. As previously reported [62], both male and female WT mice in their mature-adult age stayed longer on the rotarod than in middle-aged, confirming the disadvantage of aging on motor function, and the specificity of the test. This aging effect was also observed in male and female cKO mice. However, no significant difference of falling latency was found between WT and cKO mice, regardless of sex and age (Fig. 7A). Consistently, no difference of grip strength was found in male or female, mature-adult or middle-aged WT and cKO mice (Fig. 7B). These results appear to suggest that the motor function is not, if any, affected as dominantly as the chronic pain response in cKO mice.

Discussion

JMJD3 is widely expressed in a variety of cell types within and without the adult brain, suggesting its expression pattern, regulatory targets and cellular functions are highly cell-specific. Although a similarity of JMJD3 expression was found within the major groups of TH+CA neurons in adult mouse brain (Fig. 1A-C), the functional diversity of JMJD3 between different groups was at least revealed by the region-specific reduction of DA contents in the midbrain and striatum of cKO and GSK-J4 mice (Fig. 2). Despite of the meso-striatal loss of DA in mDA neurons, the effects of JMJD3 deficiency in other TH+cell groups remain elusive. For instance, the cytoplasmic expression of JMJD3 in TH+C-LTMR neurons of DRG (Fig. 1D), which are regarded as non-DA phenotype [49] suggests alternative functions and mechanisms of JMJD3, such as demethylating non-histone targets [63].

Adult mDA neurons regulate DA levels via multiple manners including DA biosynthesis. The reduced expression of TH by loss of JMJD3 has confirmed the disruption of DA biosynthesis to be one of, if not all, the major causes leading to DA loss in cKO midbrain. This conclusion is further supported by the finding of concurrent reduction of NURR1 expression in the same place (Fig. 3). However, NURR1 is also a master regulator of several other DA phenotype genes such as *Slc18a2* and *Slc6a3*, encoding vesicular monoamine transporter 2 and DA transporter, respectively [23, 64]. It remains unclear whether the vesicular release and re-uptake of DA are affected by JMJD3.

The involvement of JMJD3 in both mDA progenitors [26] and adult mDA neurons collectively suggest demethylated H3K27 as a foundational epigenetic mark for TH expression throughout the developmental fate of mDA neurons. The structural and functional similarities shared by JMJD3 and another H3K27me3 demethylase UTX [28] raise the question of whether compensational effect exists for JMJD3 deficiency. Because the biochemical and behavioral outcomes from cKO and GSK-J4 are highly consistent, it appears to suggest that most of these effects are attributable to JMJD3. In fact, a number of comparative studies have demonstrated that their functions are not always overlapping, depending on cell types and expression levels [65–69]. However, the possible involvement of UTX cannot be completely excluded. As GSK-J4 also inhibits UTX [51, 70], this question might be explained in future by exploring the additional effects of GSK-J4 on *Jmjd3* cKO mice.

Both cKO and systemic GSK-J4 injection cause reduced DA level in midbrain. Moreover, temporary GSK-J4 injection right before pain recovery causes similar pain behavior as cKO (Figs. 5 and 6). These results support an analgesia role of mDA in chronic pain. This conclusion is consistent with previous studies showing

that neurotoxin-induced depletion of mDA neurotransmission attenuates psychostimulant-evoked analgesia [17, 18]. Conversely, recent studies have reported chronic pain as a reducer of DA content in VTA DA neurons [9, 11, 71], likely suggesting a feedback loop between mDA and the central modulation of chronic pain. Clinically, psychostimulants such as amphetamine and cocaine elicit analgesia and rewarding effects, both of which involve VTA DA activity [72]. Whether manipulation of JMJD3 affect drug addiction-related behaviors remains an intriguing question for future investigation.

Regardless of cKO, the middle-aged mice of both sexes have exhibited marked prolonged hyperalgesia in comparison to mature-adult ones (Fig. 5B-E), suggesting an age-dependent pain chronification. Interestingly, the mDA system is widely accepted to be compromised in aging brain [73–75]. It is likely that the prolonged hyperalgesia in older mice is, at least partially, due to attenuated DA level in midbrain. Indeed, our preliminary experiment has confirmed that not only TH, but also NURR1 and JMJD3 are less expressed in male middle-aged mouse midbrains (unpublished data), suggesting a weakened DA biosynthesis pathway along aging. It would be interesting to test whether antagonizing the progression of this pathway attenuate age-related prolonged hyperalgesia.

Roughly 15% of DRG neurons express TH and TH mRNA is expressed in about 40% of mouse L4-6 C-LTMRs [76]. These peripheral nociceptive neurons play an integral part in transducing low-threshold mechanical stimuli in normal conditions or nociceptive stimuli in inflammatory conditions, which could be affected by systemic injection of GSK-J4. However, the effect from C-LTMRs has been circumvented by the focal injection of GSK-J4 in L3-L5 (Fig. 6). Although JMJD3 plays a significant role in neuroinflammation that might affect mechanical hyperalgesia, inhibition of JMJD3 usually leads to attenuation of inflammation and the cells that execute this function mostly do not express TH [31, 32, 34].

A high consistency of CA content changes is observed between drug-induced global JMJD3 inhibition and *Jmjd3* cKO (Fig. 2A, C). Moreover, the chronic hyperalgesia effect was remarkably strong following only 2 days of i.p. injection of GSK-J4 (Fig. 6). This provides supportive evidence for utilizing GSK-J4 as an unbiased tool for investigating roles of JMJD3 in the brain. On the other hand, recent studies suggest promising potential of JMJD3 inhibitors in cancer therapy. For instance, GSK-J4 exhibits high efficiency in targeting pediatric brainstem glioma and high-risk neuroblastoma [70, 77]. However, our results show that the i.p. injection of GSK-J4 would have remarkable impact on the metabolism of mDA system in adult mouse brain. The adverse effects of targeting JMJD3 on mDA-related functions and behaviors in preclinical and clinical trials deserve more attention.

It is obvious that the reductions of TH expression and DA levels are not due to neurotoxicity, as no signs of cell death or loss of mDA neurons are observed in either SNc or VTA of cKO or GSK-J4 mice. This is largely distinguished from the neurotoxic characteristics commonly found in PD [78]. The discrepancy is further supported by the fact that no behavioral difference was found from cKO mice in the accelerating rotarod test and grip strength test, both of which are commonly used to assess motor dysfunction in rodent models of PD [61]. Although it is possible that difference might exist in other more delicate tests for locomotor activity, we conclude in the current stage that the impairment of motor function is not one major behavioral consequence of JMJD3 deficiency.

Supplementary Information

The online version contains supplementary material available at https://doi.org/10.1186/s40478-024-01912-x.

Supplementary Figure 1: Validation of Jmjd3 conditional knockout (cKO) mice. (**A**) Genetic DNAs were extracted from tails of mice and applied to semi-quantitative PCR analysis to verify the loci carrying *Th*-CRE and *Jmjd3* loxP sequences using specific primers. A schematic of primer positions spanning the exons 21 and 22 of *Jmjd3* and loxP allele is shown. Mice carrying one band by *Th*-CRE primer and two bands by loxP primer represent cKO and mice carrying one band by CRE primer and one band near 300 bp by loxP primer represent control genotype (WT). (**B**) Representative immunofluorescence images of the JMJD3 expression in tyrosine hydroxylase (TH) + midbrain DA neurons in WT and cKO mice. Cell nuclei were counterstained by 4',6-diamidino-2-phenylindole (DAPI). Scale bar represents 50 µm. (**C**) Western blot analysis and quantification of JMJD3 expression in the ventral midbrains of WT and cKO mice. Each lane represents one mouse. GAPDH was used as an internal control. Data represent mean ± SEM. $^{*}P < 0.05$; Student's t-test

Supplementary Figure 2: Dopamine (DA) and norepinephrine (NE) levels in different brain regions of 4-month-old female Jmjd3 conditional knockout (cKO) and control littermate (WT) mice. Brain regions include frontal cortex (CTX), striatum (STRM), midbrain (MB), cerebellum (CB) and medulla oblongata (MO). $N = 4–7$ mice. Data represent mean ± SEM. $^{*}P < 0.05$, Student's t-test

Supplementary Figure 3: Morphology and cell status in the midbrain of Jmjd3 conditional knockout (cKO) mice. Representative images of 4',6-diamidino-2-phenylindole (DAPI) staining of the ventral tegmental area (VTA), substantia nigra pars compacta (SNc) and pars reticulata (SNr) from (**A**) cKO mice and their control littermates (WT) and (**B**) GSK-J4-injected mice and their control (Vehicle). DAPI is used to assess the morphology of cell nuclei and the compactness of tissue. No cell nucleus condensation or abnormal morphologies such as disordered arrangement or missing interspaces were observed in cKO and GSK-J4 in comparison to WT and Vehicle, respectively. Scale bar represents 100 µm

Supplementary Figure 4: Effects of JMJD3 inhibition on TH expression in vitro. (**A**) Representative immunofluorescence images and quantification of tyrosine hydroxylase (TH) + cells in MES23.5 DA neuronal cell line culture with or without treatment of JMJD3 inhibitor GSK-J4. (**B**) Real-time PCR analysis of *Th* mRNA expression in response to different doses of GSK-J4 treatment. (**C**) Quantification of TH + cell number in primary mouse DA neuronal cell culture underwent short hairpin RNA-mediated JMJD3 knockdown (sh-JMJD3) or control (plko.1). (**D**) Real-time PCR analysis confirmed that mRNA levels of *Jmjd3*, *Utx* and *Th* were affected by sh-JMJD3. Cell numbers were counted in 10 random areas of each culture coverslip

using an eyepiece grid at a magnification ×100. (**E**) Representative immunofluorescence images showing TH expression in NURR1-overexpressing MES23.5 cells underwent GSK-J4 treatment or sh-JMJD3. Scale bar represents 100 μm. $N = 3$ independent cell cultures. Data represent mean ± SEM. *$P < 0.05$; one-way ANOVA with Tukey's post-hoc test

Supplementary Figure 5: Verification of focal inhibition of JMJD3. Western blot analysis was performed to assess the level of histone 3 lysine 27 trimethylation (H3K27me3) in the tissues extracted from lumbar spinal cords and corresponding DRGs 2 h after intrathecal injection of GSK-J4. Level of histone 3 (H3) was used as an internal control. Each lane represents one mouse

Supplementary Figure 6: Basal mechanical hyperalgesia (**A**) and thermal hyperalgesia (**B**) of Jmjd3 conditional knockout (cKO) mice and their control littermates (WT). $N = 4–7$ mice. Data represent mean ± SEM. Ns = not significant, Student's t-test

Supplementary Table 1: (**A**) Antibody and drug information. (**B**) The parameters for multiple reaction monitoring (MRM). (**C**) Primers for genotyping and quantitative PCR analysis

Supplementary Figure 7: Original figures of immunoblots

Acknowledgements
We thank Dr. Degui Charlie Chen and Dr. Fiona E. Harrison for providing *Jmjd3* loxP mice and *Svct2* KO embryos.

Author contributions
XBH designed the study, performed the cell and animal experiments, analyzed the data, and wrote the paper. FG performed the cell and animal experiments, analyzed the data, and drafted the manuscript. WZ performed HPLC-MS experiments, analyzed the data, and drafted the manuscript. WL provided Th-CRE mice, MES23.5 cell line, and provided administrative support. JF performed the animal experiments, analyzed the data and prepared the figures. QC performed the animal experiments and analyzed the data. YM, YZ and YW analyzed the data and prepared the figures. SHL provided technical support for Svct2 KO-related experiments. HJW provided technical support for pain-related animal experiments. QZ helped generate the mouse models. RY performed the western blot experiments. All authors have approved the final version of the manuscript.

Funding
XBH is supported by the National Natural Science Foundation of China (31701287). FG is supported by the National Natural Science Foundation of China (32100779).

Data availability
No datasets were generated or analysed during the current study.

Declarations

Competing interests
The authors declare no competing interests.

Ethics approval
Approval was obtained from the ethics committee of Shanghai University of Medicine & Health Sciences. The procedures used in this study adhere to the tenets of the Declaration of Helsinki.

Consent to participate
Not applicable.

Consent to publish
Not applicable.

Received: 25 September 2024 / Accepted: 9 December 2024
Published online: 23 December 2024

References

1. Garritsen O, Van Battum EY, Grossouw LM, Pasterkamp RJ (2023) Development, wiring and function of dopamine neuron subtypes. Nat Rev Neurosci 24:134–152
2. Björklund A, Dunnett SB (2007) Dopamine neuron systems in the brain: an update. Trends Neurosci 30:194–202
3. Willemsen MA, Verbeek MM, Kamsteeg E-J, de Rijk-van Andel JF, Aeby A, Blau N et al (2010) Tyrosine hydroxylase deficiency: a treatable disorder of brain catecholamine biosynthesis. Brain 133:1810–1822
4. Zhou Q-Y, Quaife CJ, Palmiter RD (1995) Targeted disruption of the tyrosine hydroxylase gene reveals that catecholamines are required for mouse fetal development. Nature 374:640–643
5. Korner G, Noain D, Ying M, Hole M, Flydal MI, Scherer T et al (2015) Brain catecholamine depletion and motor impairment in a *th* knock-in mouse with type B tyrosine hydroxylase deficiency. Brain 138:2948–2963
6. Vecchio LM, Sullivan P, Dunn AR, Bermejo MK, Fu R, Masoud ST et al (2021) Enhanced tyrosine hydroxylase activity induces oxidative stress, causes accumulation of autotoxic catecholamine metabolites, and augments amphetamine effects in vivo. J Neurochem 158:960–979
7. Guo D, Zhang S, Sun H, Xu X, Hao Z, Mu C et al (2018) Tyrosine hydroxylase down-regulation after loss of Abelson helper integration site 1 (AHI1) promotes depression via the circadian clock pathway in mice. J Biol Chem 293:5090–5101
8. Johnson ME, Salvatore MF, Maiolo SA, Bobrovskaya L (2018) Tyrosine hydroxylase as a sentinel for central and peripheral tissue responses in Parkinson's progression: evidence from clinical studies and neurotoxin models. Prog Neurobiol 165–167:1–25
9. Yang H, de Jong JW, Cerniauskas I, Peck JR, Lim BK, Gong H et al (2021) Pain modulates dopamine neurons via a spinal–parabrachial–mesencephalic circuit. Nat Neurosci 24:1402–1413
10. Markovic T, Pedersen CE, Massaly N, Vachez YM, Ruyle B, Murphy CA et al (2021) Pain induces adaptations in ventral tegmental area dopamine neurons to drive anhedonia-like behavior. Nat Neurosci 24:1601–1613
11. Huang S, Zhang Z, Gambeta E, Xu SC, Thomas C, Godfrey N et al (2020) Dopamine inputs from the Ventral Tegmental Area into the Medial Prefrontal Cortex modulate Neuropathic Pain-Associated behaviors in mice. Cell Rep 31:107812
12. Martikainen IK, Nuechterlein EB, Pecina M, Love TM, Cummiford CM, Green CR et al (2015) Chronic back Pain is Associated with alterations in dopamine neurotransmission in the Ventral Striatum. J Neurosci 35:9957–9965
13. Scott DJ, Heitzeg MM, Koeppe RA, Stohler CS, Zubieta J-K (2006) Variations in the Human Pain stress experience mediated by ventral and dorsal basal ganglia dopamine activity. J Neurosci 26:10789–10795
14. Hnasko TS, Sotak BN, Palmiter RD (2005) Morphine reward in dopamine-deficient mice. Nature 438:854–857
15. Ossipov MH, Dussor GO, Porreca F (2010) Central modulation of pain. J Clin Invest 120:3779–3787
16. Taylor AMW, Becker S, Schweinhardt P, Cahill C (2016) Mesolimbic dopamine signaling in acute and chronic pain: implications for motivation, analgesia, and addiction. Pain 157:1194–1198
17. Altier N, Stewart J (1999) The role of dopamine in the nucleus accumbens in analgesia. Life Sci 65:2269–2287
18. Wood PB (2008) Role of central dopamine in pain and analgesia. Expert Rev Neurother 8:781–797
19. Hipolito L, Wilson-Poe A, Campos-Jurado Y, Zhong E, Gonzalez-Romero J, Virag L et al (2015) Inflammatory Pain promotes increased opioid Self-Administration: role of dysregulated ventral Tegmental Area opioid receptors. J Neurosci 35:12217–12231
20. Taylor AMW, Castonguay A, Taylor AJ, Murphy NP, Ghogha A, Cook C et al (2015) Microglia disrupt mesolimbic reward circuitry in Chronic Pain. J Neurosci 35:8442–8450
21. Beiske AG, Loge JH, Rønningen A, Svensson E (2009) Pain in Parkinson's disease: prevalence and characteristics. Pain 141:173–177
22. Lenartowski R, Goc A (2011) Epigenetic, transcriptional and posttranscriptional regulation of the tyrosine hydroxylase gene. Int j dev Neurosci 29:873–883
23. van Heesbeen HJ, Mesman S, Veenvliet JV, Smidt MP (2013) Epigenetic mechanisms in the development and maintenance of dopaminergic neurons. Development 140:1159–1169
24. He X-B, Guo F, Li K, Yan J, Lee S-H (2022) Timing of MeCP2 expression determines midbrain dopamine neuron phenotype specification. Stem Cells. sxac061

25. He X-B, Yi S-H, Rhee Y-H, Kim H, Han Y-M, Lee S-H et al (2011) Prolonged membrane depolarization enhances midbrain dopamine neuron differentiation via epigenetic histone modifications. Stem Cells 29:1861–1873
26. He X-B, Kim M, Kim S-Y, Yi S-H, Rhee Y-H, Kim T et al (2015) Vitamin C facilitates dopamine neuron differentiation in fetal midbrain through TET1- and JMJD3-Dependent Epigenetic Control Manner: Epigenetic Control of mDA Neuron Development by VC. Stem Cells 33:1320–1332
27. Yi S-H, He X-B, Rhee Y-H, Park C-H, Takizawa T, Nakashima K et al (2014) Foxa2 acts as a co-activator potentiating expression of the Nurr1-induced DA phenotype via epigenetic regulation. Development 141:761–772
28. Hong S, Cho Y-W, Yu L-R, Yu H, Veenstra TD, Ge K (2007) Identification of JmjC domain-containing UTX and JMJD3 as histone H3 lysine 27 demethylases. Proceedings of the National Academy of Sciences. 104:18439–44
29. Agger K, Cloos PAC, Christensen J, Pasini D, Rose S, Rappsilber J et al (2007) UTX and JMJD3 are histone H3K27 demethylases involved in HOX gene regulation and development. Nature 449:731–734
30. Sen GL, Webster DE, Barragan DI, Chang HY, Khavari PA (2008) Control of differentiation in a self-renewing mammalian tissue by the histone demethylase JMJD3. Genes Dev 22:1865–1870
31. Alexaki VI, Fodelianaki G, Neuwirth A, Mund C, Kourgiantaki A, Ieronimaki E et al (2018) DHEA inhibits acute microglia-mediated inflammation through activation of the TrkA-Akt1/2-CREB-Jmjd3 pathway. Mol Psychiatry 23:1410–1420
32. De Santa F, Totaro MG, Prosperini E, Notarbartolo S, Testa G, Natoli G (2007) The histone H3 Lysine-27 demethylase Jmjd3 links inflammation to inhibition of polycomb-mediated gene silencing. Cell 130:1083–1094
33. Przanowski P, Dabrowski M, Ellert-Miklaszewska A, Kloss M, Mieczkowski J, Kaza B et al (2014) The signal transducers Stat1 and Stat3 and their novel target Jmjd3 drive the expression of inflammatory genes in microglia. J Mol Med 92:239–254
34. Tang Y, Li T, Li J, Yang J, Liu H, Zhang XJ et al (2014) Jmjd3 is essential for the epigenetic modulation of microglia phenotypes in the immune pathogenesis of Parkinson's disease. Cell Death Differ 21:369–380
35. Jia W, Wu W, Yang D, Xiao C, Su Z, Huang Z et al (2018) Histone demethylase JMJD3 regulates fibroblast-like synoviocyte-mediated proliferation and joint destruction in rheumatoid arthritis. FASEB J 32:4031–4042
36. Svotelis A, Bianco S, Madore J, Huppé G, Nordell-Markovits A, Mes-Masson A-M et al (2011) H3K27 demethylation by JMJD3 at a poised enhancer of anti-apoptotic gene BCL2 determines ERα ligand dependency. EMBO J 30:3947–3961
37. Barradas M, Anderton E, Acosta JC, Li S, Banito A, Rodriguez-Niedenfuhr M et al (2009) Histone demethylase JMJD3 contributes to epigenetic control of INK4a/ARF by oncogenic RAS. Genes Dev 23:1177–1182
38. Agger K, Cloos PAC, Rudkjaer L, Williams K, Andersen G, Christensen J et al (2009) The H3K27me3 demethylase JMJD3 contributes to the activation of the INK4A-ARF locus in response to oncogene- and stress-induced senescence. Genes Dev 23:1171–1176
39. Burchfield JS, Li Q, Wang HY, Wang R-F (2015) JMJD3 as an epigenetic regulator in development and disease. Int J Biochem Cell Biol 67:148–157
40. Zhang X, Liu L, Yuan X, Wei Y, Wei X (2019) JMJD3 in the regulation of human diseases. Protein Cell 10:864–882
41. Flurkey K, Mcurrer J, Harrison D Mouse Models in Aging Research. The Mouse in Biomedical Research. Elsevier; 2007 [cited 2024 Jan 11]. pp. 637–72. https://linkinghub.elsevier.com/retrieve/pii/B9780123694546500741
42. Pu T, Mei Z, Zhang W, Liang W, Zhou X, Liang J et al (2020) An in vitro DNA phosphorothioate modification reaction. Mol Microbiol 113:452–463
43. Sun W, Shi J, Hong J, Zhao G, Wang W, Zhang D et al (2022) Natural variation and underlying genetic loci of γ-oryzanol in Asian cultivated rice seeds. The Plant Genome. [cited 2022 Aug 20]; https://onlinelibrary.wiley.com/doi/https://doi.org/10.1002/tpg2.20201
44. Hu Z, Cooper M, Crockett DP, Zhou R (2004) Differentiation of the midbrain dopaminergic pathways during mouse development. J Comp Neurol 476:301–311
45. La Manno G, Gyllborg D, Codeluppi S, Nishimura K, Salto C, Zeisel A et al (2016) Molecular Diversity of Midbrain Development in Mouse, Human, and stem cells. Cell 167:566–580e19
46. Wang H, Heijnen CJ, van Velthoven CTJ, Willemen HLDM, Ishikawa Y, Zhang X et al (2013) Balancing GRK2 and EPAC1 levels prevents and relieves chronic pain. J Clin Invest 123:5023–5034
47. Chaplan SR, Bach FW, Pogrel JW, Chung JM, Yaksh TL (1994) Quantitative assessment of tactile allodynia in the rat paw. J Neurosci Methods 53:55–63
48. Hargreaves K, Dubner R, Brown F, Flores C, Joris J (1988) A new and sensitive method for measuring thermal nociception in cutaneous hyperalgesia. Pain 32:77–88
49. Brumovsky P, Villar MJ, Hökfelt T (2006) Tyrosine hydroxylase is expressed in a subpopulation of small dorsal root ganglion neurons in the adult mouse. Exp Neurol 200:153–165
50. Li L, Rutlin M, Abraira VE, Cassidy C, Kus L, Gong S et al (2011) The Functional Organization of cutaneous low-threshold mechanosensory neurons. Cell 147:1615–1627
51. Kruidenier L, Chung C, Cheng Z, Liddle J, Che K, Joberty G et al (2012) A selective jumonji H3K27 demethylase inhibitor modulates the proinflammatory macrophage response. Nature 488:404–408
52. Zetterström RH (1997) Dopamine Neuron Agenesis in Nurr1-Deficient mice. Science 276:248–250
53. Saucedo-Cardenas O, Quintana-Hau JD, Le WD, Smidt MP, Cox JJ, Mayo FD et al (1998) Nurr1 is essential for the induction of the dopaminergic phenotype and the survival of ventral mesencephalic late dopaminergic precursor neurons. Proceedings of the National Academy of Sciences. 95:4013–8
54. Kadkhodaei B, Ito T, Joodmardi E, Mattsson B, Rouillard C, Carta M et al (2009) Nurr1 is required for maintenance of maturing and adult midbrain dopamine neurons. J Neurosci 29:15923–15932
55. Kadkhodaei B, Alvarsson A, Schintu N, Ramskold D, Volakakis N, Joodmardi E et al (2013) Transcription factor Nurr1 maintains fiber integrity and nuclear-encoded mitochondrial gene expression in dopamine neurons. Proc Natl Acad Sci 110:2360–2365
56. Crawford GD, Le WD, Smith RG, Xie WJ, Stefani E, Appel SH (1992) A novel N18TG2 x mesencephalon cell hybrid expresses properties that suggest a dopaminergic cell line of substantia nigra origin. J Neurosci 12:3392–3398
57. Song Q, Wei A, Xu H, Gu Y, Jiang Y, Dong N et al (2024) An ACC–VTA–ACC positive-feedback loop mediates the persistence of neuropathic pain and emotional consequences. Nat Neurosci. [cited 2024 Jan 11]; https://www.nature.com/articles/s41593-023-01519-w
58. Shiotsuki H, Yoshimi K, Shimo Y, Funayama M, Takamatsu Y, Ikeda K et al (2010) A rotarod test for evaluation of motor skill learning. J Neurosci Methods 189:180–185
59. Liang B, Zhang L, Zhang Y, Werner CT, Beacher NJ, Denman AJ et al (2022) Striatal direct pathway neurons play leading roles in accelerating rotarod motor skill learning. iScience 25:104245
60. Bohlen M, Cameron A, Metten P, Crabbe JC, Wahlsten D (2009) Calibration of rotational acceleration for the rotarod test of rodent motor coordination. J Neurosci Methods 178:10–14
61. Brooks SP, Dunnett SB (2009) Tests to assess motor phenotype in mice: a user's guide. Nat Rev Neurosci 10:519–529
62. Shoji H, Takao K, Hattori S, Miyakawa T (2016) Age-related changes in behavior in C57BL/6J mice from young adulthood to middle age. Molecular Brain. [cited 2018 Apr 15];9. http://www.molecularbrain.com/content/9/1/11
63. Zhao L, Zhang Y, Gao Y, Geng P, Lu Y, Liu X et al (2015) JMJD3 promotes SAHF formation in senescent WI38 cells by triggering an interplay between demethylation and phosphorylation of RB protein. Cell Death Differ 22:1630–1640
64. Ang S-L (2006) Transcriptional control of midbrain dopaminergic neuron development. Development 133:3499–3506
65. Dai J, Lu J, Zhang Y, Shen Y (2010) Jmjd3 activates *Mash1* gene in RA-induced neuronal differentiation of P19 cells. J Cell Biochem 110:1457–1463
66. Burgold T, Spreafico F, De Santa F, Totaro MG, Prosperini E, Natoli G et al (2008) B Sullivan editor. The histone H3 lysine 27-Specific demethylase Jmjd3 is required for neural commitment. PLoS ONE 3 e3034
67. Shan Y, Zhang Y, Zhao Y, Wang T, Zhang J, Yao J et al (2020) JMJD3 and UTX determine fidelity and lineage specification of human neural progenitor cells. Nat Commun 11:382
68. Kawaguchi A, Ochi H, Sudou N, Ogino H (2012) Comparative expression analysis of the H3K27 demethylases, JMJD3 and UTX, with the H3K27 methylase, EZH2, in Xenopus. Int J Dev Biol 56:295–300
69. Manna S, Kim JK, Baugé C, Cam M, Zhao Y, Shetty J et al (2015) Histone H3 lysine 27 demethylases Jmjd3 and utx are required for T-cell differentiation. Nat Commun 6:8152
70. Hashizume R, Andor N, Ihara Y, Lerner R, Gan H, Chen X et al (2014) Pharmacologic inhibition of histone demethylation as a therapy for pediatric brainstem glioma. Nat Med 20:1394–1396
71. Vergara F, Sardi NF, Pescador AC, Guaita GO, Jark Stern CA, Chichorro JG et al (2020) Contribution of mesolimbic dopamine and kappa opioid systems to the transition from acute to chronic pain. Neuropharmacology 178:108226

72. Morales M, Margolis EB (2017) Ventral tegmental area: cellular heterogeneity, connectivity and behaviour. Nat Rev Neurosci 18:73–85
73. Dreher J-C, Meyer-Lindenberg A, Kohn P, Berman KF (2008) Age-related changes in midbrain dopaminergic regulation of the human reward system. Proc Natl Acad Sci USA 105:15106–15111
74. Grady C (2012) The cognitive neuroscience of ageing. Nat Rev Neurosci 13:491–505
75. Samanez-Larkin GR, Knutson B (2015) Decision making in the ageing brain: changes in affective and motivational circuits. Nat Rev Neurosci 16:278–289
76. Usoskin D, Furlan A, Islam S, Abdo H, Lönnerberg P, Lou D et al (2015) Unbiased classification of sensory neuron types by large-scale single-cell RNA sequencing. Nat Neurosci 18:145–153
77. Lochmann TL, Powell KM, Ham J, Floros KV, Heisey DAR, Kurupi RIJ et al (2018) Targeted inhibition of histone H3K27 demethylation is effective in high-risk neuroblastoma. Sci Transl Med 10:eaao4680
78. Meredith GE, Sonsalla PK, Chesselet M-F (2008) Animal models of Parkinson's disease progression. Acta Neuropathol 115:385–398

Publisher's note